Advances in Geo-Energy Research

Vol. 21, No. 1, p. 29-41, 2026

Original article

Mineral interphases control the thermal weakening and strengthening of granite

Wilson F. Espinoza[1,2], Timothy J. Kneafsey[3], Jean-Michel Pereira[4], Aryong Yun[2], Sheng C. Dai[2]*

[1]*College of Science and Engineering, Texas State University, San Marcos 78666, USA*

[2]*School of Civil and Environmental Engineering, Georgia Institute of Technology, Atlanta 30332, USA*

[3]*Energy Geosciences Division, Lawrence Berkeley National Laboratory, Berkeley 94720, USA*

[4]*Navier, Ecole des Ponts, Univ Gustave Eiffel, CNRS, Marne-la-Vallée 77201, France*

Keywords:
Granite
mineral interphase
temperature
indentation
geothermal

Cited as:
Espinoza, W. F., Kneafsey, T. J., Pereira, J. -M., Yun, A., Dai, S. C. Mineral interphases control the thermal weakening and strengthening of granite. Advances in Geo-Energy Research, 2026, 21(1): 29-41. https://doi.org/10.46690/ager.2026.07.05

Abstract:
While existing studies on hot rocks across various scales have provided valuable insights, they have yet to offer mechanistic explanations at the mineral level for the controversy in temperature-dependent changes in the granite mechanical properties. Most prior work, moreover, relies on samples that are heated and then cooled before testing, a step that relaxes thermal stresses and may introduce cooling-induced microcracks. Unlike these cooled-then-tested measurements, this study examines mineral-to-mineral interactions in granites recovered from two geothermal sites of contrasting mineralogy, at elevated temperatures using instrumented nanoindentation. The findings indicate that temperature causes predominantly inter- rather than intra-mineral changes in granite. Interphases of minerals with different strengths and coefficients of thermal expansion, like quartz-biotite and albite-biotite, degrade as temperature increases, whereas interphases between minerals with similar mechanical and thermal properties, like quartz-albite, are strengthened by temperature. Granite properties at elevated temperatures therefore result from a competition between thermal degradation in mismatching mineral interphases and thermal strengthening of interphases of comparable minerals. This competition leads to an overall thermal degradation in biotite-rich granite, but thermal strengthening in quartz- and albite-rich granite, and thus, the dominant interphase type set by the mineral assemblage governs whether a given granite weakens or strengthens. These interphase-controlled mechanisms reconcile the conflicting weakening and strengthening behaviors reported for granite and inform the prediction of crystalline-rock performance in enhanced geothermal systems.

1. Introduction

Crystalline rocks like granite are well suited for enhanced geothermal systems due to their high strength and low permeability (Wyborn et al., 2004; Zhang et al., 2018; Hill et al., 2022) and radioactive waste disposal (Glatz et al., 1995; Gibb and Attrill, 2003; Yang et al., 2017; Yin et al., 2020) facilities. The successful deployment of these systems depends on enhanced understanding and technologies to characterize, monitor, and predict the behavior of hot crystalline rocks during the drilling, construction, operation, and decommissioning phases (Yin et al., 2016; Kumari et al., 2017; Gautam et al., 2018; Hu et al., 2018).

The elastic modulus of granite shows a pronounced decline at temperatures of approximately ~400-600 °C (Chen et al., 2012; Shao et al., 2015; Singh et al., 2015). The tensile and compressive strengths of granite typically decrease with increasing temperature; however, some literature reports an initial increase upon heating up to approximately 300 °C

Yandy Scientific Press

*Corresponding author.
E-mail address: acy28@txstate.edu (W. Espinoza); tjkneafsey@lbl.gov (T. Kneafsey); jean-michel.pereira@enpc.fr (J. Pereira); aryong.yun@gatech.edu (A. Yun); sdai6@gatech.edu (S. Dai).

Received April 25, 2026; revised May 22, 2026; accepted June 15, 2026; available online June 17, 2026.

followed by strength decrease with increasing temperatures (Török and Török, 2015; Gautam et al., 2018; Kumari et al., 2019). Such controversial observations have not been satisfactorily explained (Géraud et al., 1992; Dwivedi et al., 2008; Gómez-Heras et al., 2008; Wong et al., 2020). In addition, temperature increases the density of fractures and crack growth velocity in granite (Atkinson, 1980). Based on acoustic emissions observations, quartz-rich rocks increase ductility with temperature, yet, exhibit brittle failure as peak strength is approached (Peng and Yang, 2018). Thermal cycling treatments are less effective under prolonged constant-temperature conditions in inducing severe fracture-driven rock instability (Inserra et al., 2013; Yin et al., 2016; Feng et al., 2019).

Considerably scattered data on temperature effects on granite has triggered further small-scale analyses. Some studies have indirectly associated mineral interactions with mesoscale material properties using acoustic emission monitoring (Wang et al., 1989; Griffiths et al., 2018; Kumari et al., 2019), X-ray micro-CT observations (Yang et al., 2017; Talukdar et al., 2018), and wave velocity measurements (Wang et al., 1989; Lin, 2002; Griffiths et al., 2018). As such, with temperature rise, mild porosity reductions have been related to mineral expansion; while drastic porosity increments to the progression of mineral defects enhancing fracture connectivity. Such transitioning mechanisms tend to occur at around 300 °C within granite structures (Géraud et al., 1992; Sun et al., 2015; Yang et al., 2017). Permeability increments due to high temperature have been explained by thermal inter- and intra- granular microcracking (Darot et al., 1992; David et al., 1999; Nasseri et al., 2007; Wang et al., 2013), resulting from stress build up among minerals with heterogeneous thermal expansion (Kranz, 1983). Thus, improved flow properties of thermally treated granites have inevitably shown reduced strength and stiffness (Yin et al., 2016; Gautam et al., 2018; Hu et al., 2018). Stress concentrations have been identified as the main mechanism inducing fracturing in granites due to the geometrical heterogeneity of its minerals, which also contain irregular and dissimilar defects (Li et al., 2022). Moreover, given that thermal stresses can overcome inter-mineral strength and particle cohesion, fractures can grow to destroy granite structures (Dwivedi et al., 2008; Wang and Konietzky, 2022). Thermo-mechanical models based on laboratory-induced fracture networks in granites have shown that high temperature induces crack nucleation, which peaks at the alpha-beta transition of quartz (~573 °C) (David et al., 2012; Wang et al., 2013; Xu and Karakus, 2018; Wang and Konietzky, 2022).

Recent findings have also shown microcracks initiate at 300 °C and coalesce around 400-600 °C using experimental and numerical approaches (Xu et al., 2023). Other numerical models highlight the profound influences of micro-fracturing processes on rock strength. Under low confining environments, fracturing is initially dominated by spalling and splitting mechanisms driven by mineral contrast, which trigger localized tensile microcracking that progressively coalesces and, with increasing confinement, transitions into shear-dominated failure (Hamdi et al., 2015; Zhao and Zhao, 2018). Discrete and finite element methods have also shown that stress concentrations, especially of the tensile type, induce granite failure by overcoming its grain boundary strength (Vázquez et al., 2015; Saksala, 2021; Wang and Konietzky, 2022). Similarly to experimental findings, numerical analyses also highlight temperature effects on granite influenced by additional factors including mineral size and volume fraction (Lan et al., 2010; Saksala, 2021; Li et al., 2022). In general, granites with smaller particles have shown improved thermal resistance and mechanical performance than their counterparts (Martin and Stimpson, 1994; Miskovsky et al., 2004; Hamdi et al., 2015). However, connections between the thermal strength of granite and the thermoelastic properties of its main constituent minerals (e.g., quartz, feldspar, and biotite) are still under discussion (Merriam et al., 1970; Shea and Kronenberg, 1993; Li et al., 2022).

Numerous investigative approaches have established a rich database capturing temperature effects on granite and other crystalline rocks using conventional mechanical testing, which are typically at scales larger than their mineral grains. These studies are limited in offering insight into the mechanistic and mineralogical origin of the temperature impacts on the change of granite behaviors. Simulations to link grain-level properties to macroscopic behaviors of granite are usually challenged by validated mineral and mineral-mineral interaction parameters, particularly at elevated temperatures. Such data are extremely rare in literature. Moreover, it is typically based on room temperature measurements of grain-contact-architectures reconstructed from thermally treated rocks. In fact, the overwhelming majority of these measurements are performed on specimens that are heated and then cooled to room temperature before testing. Cooling reverses the thermal expansion responsible for interphase stress and can itself nucleate differential-contraction microcracks, so cooled-and-tested specimens capture a thermally relaxed, damage-altered state rather than the in-situ condition; the reported sensitivities of granite properties to cooling rate and cooling medium indicate that this post-treatment step is itself a source of the observed scatter. Real-time inter- and intra-grain behaviors under temperature have been difficult to monitor (Zhou et al., 2021).

Here mechanical properties are measured in situ, at temperature, using instrumented nanoindentation, thereby preserving the thermal expansion and interphase stresses that cooled-and-tested measurements relax away and resolving the multiphase behavior of granite at the mineral grain level. This study elucidates how and to what extent the microscale mechanical properties of individual granitic minerals, i.e., albite, biotite, and quartz, as well as their interfacial interactions, could affect the variation of elastic modulus and hardness of granite with increasing temperatures. These results shed light on intra- and inter-mineral interactions of granite upon heating.

2. Experimental design

2.1 Sample description and preparation

The granite samples analyzed in this study were 38.1 mm (1.5”) diameter cores collected from the Sanford Underground

Research Facility (SURF) located in South Dakota (hereafter called SURF granite) at a depth of 47.9 m (153') and approximate in-situ temperature of 45°C , and from the Frontier Observatory for Research in Geothermal Energy (FORGE) site in Utah (i.e., Utah granite hereafter) at a depth of 1,090.6 m (3,578') and approximate temperature of 112 °C.

The samples were cut using a 0.3 mm thick precision wafer blade and subsequently polished with P800, P1200, and P2400 sandpapers (averaged grit sizes of 25.8, 15.3, and 6.5 μm, respectively). The resulting surface roughness was 0.3 μm for both samples, determined using a stylus profilometer (Veeco Dektak-8). Increased surface roughness has been shown to have only minor effect on the average elastic modulus and hardness measured by indentation, but it increases their standard deviation (Espinoza et al., 2022) ; therefore, the influence of obvious imperfections caused by surface asperities and valleys were minimized through polishing. Additionally, prior to mechanical testing, samples were inspected under optical microscopes to select indentation testing locations free of other obvious imperfections like microcracks and large pores.

2.2 Sample's mineralogy

The focus of this study is on the mineral interactions upon heating. Thus, understanding the distribution and volume fraction of the constituent granitic minerals in both granite samples are necessary. Fig. 1 show the mineralogy maps obtained using the scanning electron microscopy and dispersive X-ray spectroscopy SEM-EDS (Zeiss Ultra60) and the X-ray diffractometer XRD (PANalytical EMPYREAN). Diffraction patterns, expressed in intensity with crystal orientation, were matched to the characteristic diffraction patterns of pure constituent minerals through Rietveld refinement using HighScore Plus 4.0.

The results show that SURF granite in mainly composed of quartz (59.1%) and biotite (38.8%), with minor orthoclase (1.3%) and plagioclase (0.8%), whereas Utah granite consists of quartz (47.6%), albite (40.8%), biotite (11.4%), and negligible amounts of other minerals (0.1%). These findings highlight a substantial difference in biotite content between the two granites, both of which are dominated by quartz.

2.3 Instrumented indentation

Indentation evaluates material behavior under a loading-creep-unloading cycle using a diamond indenter. Elastic and plastic deformation occur during loading, while unloading is predominantly elastic (Oliver and Pharr, 1992; Oliver and Pharr, 2004). Key mechanical properties are derived from the unloading response and the load-depth conditions at peak load (ASTM, 2007). The elastic modulus E and hardness H of all tested specimens were calculated using the Oliver-Pharr method (Oliver and Pharr, 2004):

$$E = \left(1 - \nu_s^2\right)\left(\frac{1}{E_r} - \frac{1 - \nu_i^2}{E_i}\right)^{-1} \tag{1}$$

$$H = \frac{P_{\max}}{A_c} \tag{2}$$

where E_r is the so-called reduced elastic modulus; E_i is the elastic modulus of the indenter; ν_i is the Poisson's ratio of the indenter; ν_s is the Poisson's ratio of the testing sample; S is the sample's stiffness; $P_{\max}$ is the maximum applied force; and A_c is the projected indenter–sample contact area.

Using a Berkovich indenter, specimens were loaded from 0 to 0.1 N, followed by 20 s dwelling (at 0.1 N), and unloaded back to 0 N in this study. This maximum load was selected to probe the response of individual granite mineral phases at the microscale rather than the bulk composite response at the millimeter scale. Under these conditions, the indentation load of 0.1 N was tailored to penetrate individual mineral phases in both granites to depths smaller than 5 μm, ensuring that the plastic zones remained confined to the targeted minerals. At the same time, this depth is at least one order of magnitude larger than the measured surface roughness ($R_a \approx 0.3$ μm), which minimizes roughness-induced bias in the measured modulus and hardness and is consistent with recommendations that indentation depths be several times (i.e., > 3 times) larger than the characteristic sample roughness scale (Kim et al., 2006; Michałek et al., 2019; Espinoza et al., 2022). Both specimens are tested under temperatures of 20, 50, 100, 200, 300, and 400 °C. It should be noted that all indentation tests were performed at targeted temperature conditions, rather than on thermally treated specimens and then cooled. To accomplish it, the indenter tip was mounted in a 2 cm-long, low thermal conductivity fixture acting as both a holder and thermal separator. The indenter-holder assembly was calibrated using standard procedures on reference materials (i.e., fused quartz). The heating system incorporated thermal barriers to protect the load and depth sensors, with a fluid-circulating cooling loop maintaining low temperature at the furnace exterior while an internal heating element controlled its chamber to the target setpoints. To mitigate effects of rapid mineral dilation, the heating rate was limited to 2 °C per minute. At each temperature, 120 indentation tests were performed. Special attention was given to mitigating the effects of thermal drift by allowing the indenter and samples to reach thermal equilibrium before each temperature step (Korte et al., 2012; Sharma et al., 2025). After the furnace containing the specimens reached each target temperature, the system was held for an additional 24 h for thermal equilibrium before performing indentations at targeted temperatures (not thermally-treated-then-cooled conditions). Thermocouples attached to all samples were used to verify that the testing conditions remained constant and controlled across all experiments.

2.4 Indentation results

Each indentation test will produce the load-displacement data during loading and unloading, based on which the fundamental mechanical properties like modulus and hardness are obtained. All indentation results, i.e., the load-displacement data on the two granite samples, are summarized in Fig. 2. Each sample is tested under temperatures of 20, 50, 100, 200, 300, and 400 °C, and with 120 tests at each temperature condition. The maximum indentation depth $d_{\max}$ (corresponding to the maximum load of 100 mN) of SURF granite is 3.8 μm,

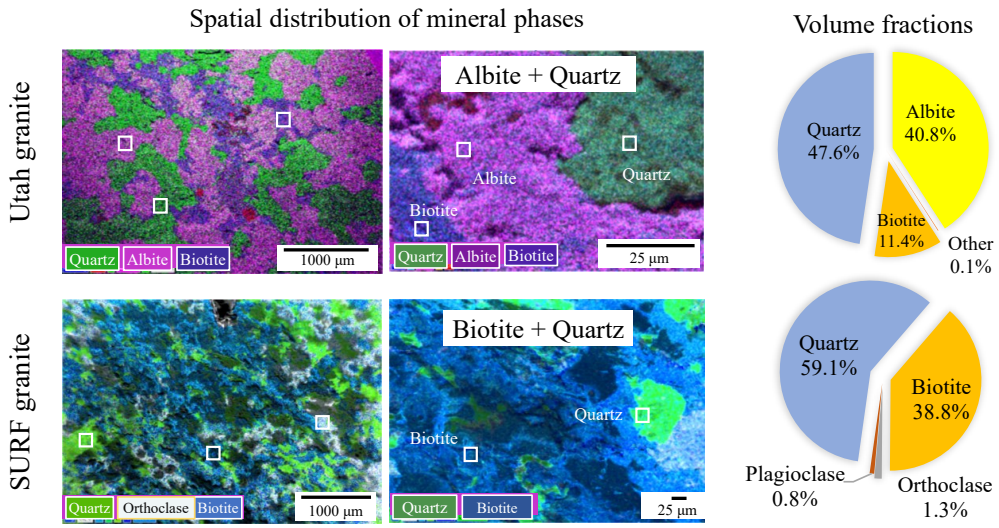

Fig. 1. Mineral phases of the Utah and SURF granites.

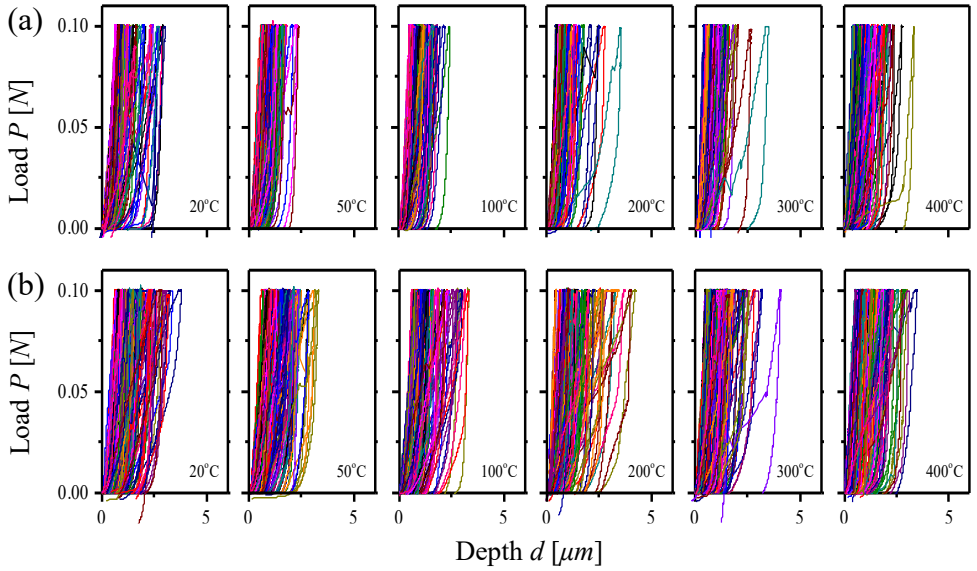

Fig. 2. Indentation signatures of (a) Utah and (b) SURF granites at 20, 50, 100, 200, 300, and 400 °C.

which is more than that of Utah granite ($d_{max} \approx 2.8$ μm) at room temperature. In general, dmax is greater in SURF granite than in Utah granite at all tested temperatures, and the load-displacement curves are more scattered for the SURF than the Utah granite. Such deformations provided the first indication of greater compliance (increased contact area in Eq. ((2))), and reduced hardness for the SURF sample with respect to the Utah granite.

To illustrate idented marks on various minerals, the mineralogy map is overlaid with squared grids. As shown in Fig. 3, each grid cell marks one indentation, and is color-coded by a legend at top: quartz Q (magenta), biotite B (blue), hornblende H (green), and plagioclase P (purple). The 'contact' and 'close contact' are grids where indentation hits on or right next to the inter-mineral boundaries. The 'cracked' are where obvious cracks are observed. A few grids are 'ignored' due to surface defects. And 'pop in' grids are where pop-in events occurred during loading. This phase and interphase classification was performed independently of the mechanical results and was used to corroborate the peak assignments obtained from the Gaussian deconvolution.

2.5 Signal deconvolution

To isolate the micromechanical contribution of mineral interphases from the bulk granite response, a deconvolution procedure in OriginPro software was employed. At each temperature, the distribution of indentation-derived elastic moduli and hardness were modeled as a sum of Gaussian components representing the main minerals (e.g., quartz, albite and biotite) and an additional component representing the quartz-albite and quartz-biotite interphases (Fig. 4). The shapes and centers of the mineral components were constrained using nanoindenta-

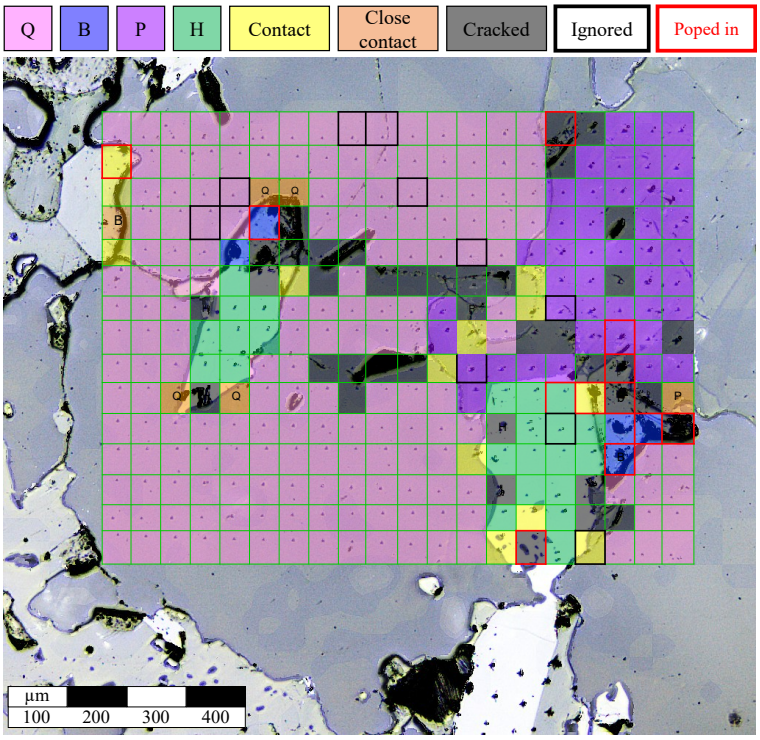

Fig. 3. Nanoindentations on different surface mineralogy.

tion data from external samples of the pure minerals (Espinoza et al., 2023), whereas the amplitudes and the interphase component parameters were obtained by nonlinear least-squares fitting (Levenberg-Marquardt) of the form:

$$y(x) = \sum_{i=1}^{N} \frac{A_i}{w_i \sqrt{\frac{\pi}{2}}} \exp\left[-2\left(\frac{x - x_{0,i}}{w_i}\right)^2\right] + y_0 \qquad (3)$$

where $y(x)$ is the measured histogram of granite elastic modulus or hardness; $x_{0,i}$ is the center of component i; w_i is its width parameter; A_i is the area of component i; and y_0 is a constant baseline accounting for a slowly varying background signal. Among these N components, two indices, denoted as $i = \text{int}, 1$ and $i = \text{int}, 2$, correspond to interphase peaks, e.g., quartz-albite and quartz-biotite.

Thus, the fitted centers $x_{0,\text{int},1}$ and $x_{0,\text{int},2}$ were taken as effective interphase properties, e.g., elastic modulus and hardness, at each temperature, whereas the remaining $x_{0,i}$ values correspond to the mineral phases. This peak-decomposition approach is consistent with the deconvolution tools implemented in OriginPro's Peak Analyzer and Multiple Peak Fit modules. In this work, the total number of components was $N = 4$ for the SURF granite and $N = 5$ for the Utah granite. These values were selected as the smallest numbers of components capable of reproducing all visually apparent peaks in the histograms while yielding acceptable coefficients of determination, $R^2 = 0.50$-0.86, and residuals without pronounced systematic structure.

To standardize the fit and capture material variability based on temperature rather than artifacts of histogram construction, all bin sizes for elastic modulus (i.e., 10 GPa) and hardness (i.e., 2 GPa) were kept uniform across temperatures. These widths were chosen as a compromise between resolution (i.e., ability to resolve distinct mineral/interphase peaks) and statistical reliability (i.e., sufficient counts per bin). For each histogram, the data as a sum of Gaussian components were modeled using the functional form in Eq. (3), using reference nanoindentation data on pure minerals to initialize peak centers and widths, which were then allowed to vary around those reference values while peak areas and interphase-related parameters were allowed to vary freely during fitting. Goodness of fit was assessed using the coefficient of determination R^2 whose values across all conditions ranged from approximately 0.5 to 0.86. Although some fits capture only the main features of the histograms and miss small shoulders or asymmetries, the tests in which the number of components or relaxed parameter constraints were varied showed that the extracted peak centers and areas change only within their reported uncertainties. It is emphasized that this Gaussian deconvolution provides an approximate rather than an exact representation of the indentation histograms. Nevertheless, the fitted peak centers and areas are stable with respect to reasonable changes in fitting constraints and thus provide a basis for extracting trend-level effective moduli and hardness values for minerals and interphases, even though the detailed histogram shapes are not perfectly reproduced.

3. Analyses and discussion

3.1 Temperature-dependent elastic modulus variations

To contrast the measured moduli at different tested temperatures, the distributions (bar chart) of measured elastic modu-

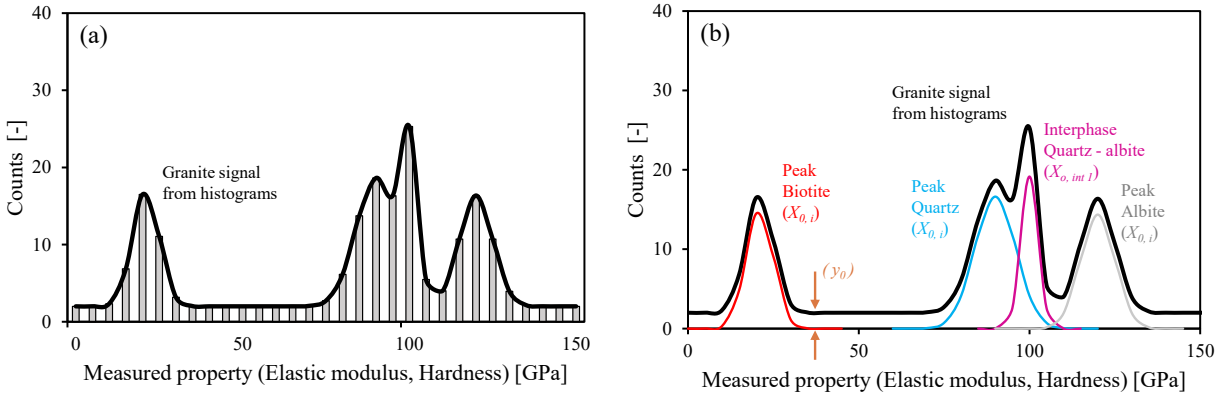

Fig. 4. Illustration of deconvolution approach using Eq. (3).

Table 1. Coefficients of variation (COV) for mineral phases and granites (descriptive statistics).

	COV elastic modulus				
Temperature (°C)	Albite	Biotite	Quartz	Utah	SURF
20	0.34	0.29	0.31	0.37	0.63
50	0.31	0.25	0.21	0.39	0.62
100	0.30	0.39	0.27	0.44	0.75
200	0.33	0.40	0.30	0.50	0.86
300	0.37	0.45	0.26	0.45	0.69
400	0.35	0.48	0.34	0.52	0.94

Table 2. Coefficients of variation (COV) for mineral phases and granites (descriptive statistics).

	COV hardness				
Temperature (°C)	Albite	Biotite	Quartz	Utah	SURF
20	0.51	0.33	0.47	0.63	0.83
50	0.50	0.57	0.37	0.62	0.81
100	0.43	0.48	0.46	0.75	0.98
200	0.54	0.42	0.50	0.86	0.91
300	0.71	0.53	0.49	0.69	0.88
400	0.47	0.52	0.63	0.94	0.82

lus for the two granite samples are summarized in Fig. 5. In general, as the temperature increases, the elastic modulus of the SURF sample decreases in both the mean value and the deviation, i.e., thermal weakening. Contrarily, that of the Utah sample increases in both mean and deviation, i.e., thermal strengthening.

Superimposed on the distribution bars are Gaussian distributions of the main constituent granitic minerals at identical temperatures. Note that the Gaussian distribution data of each constituent mineral (solid lines in Fig. 5, biotite in red; quartz in light blue, and albite in green) is from our earlier publication (Espinoza et al., 2023). To simplify the analysis, here only quartz and biotite in the SURF sample, and quartz, albite, and biotite in the Utah sample are considered, as they constitute more than 98% of the minerals in the two tested samples (Fig. 1). A Cumulative Gaussian model (colored in gold) is used to fit the bar data, comprising the distributions of each constituent mineral, as well as the Gaussians for interphases of different minerals.

The difference between the Cumulative Gaussian model and that of the individual minerals can be captured by one Gaussian distribution in the SURF sample, and two in the Utah sample. It is considered that one mineral-mineral interphase in SURF capturing the properties of the quartz-biotite (Q-B, blue-gray dashed line) interaction, and two interphases for Utah reflecting quartz-albite (Q-A, purple dashed line) and quartz/albite-biotite (Q-B or A-B, blue-gray dashed line) interactions (Fig. 5). The reason to lump Q-B and A-B into one type of Gaussian interphase in Utah, hereafter called Q–B only, mainly considers that quartz and albite have relatively close elastic moduli and hardness, which are distinctively higher than that of biotite under a given temperature condition. Therefore, the two interphases, i.e., quartz-albite (Q-A) and quartz/albite-biotite (Q-B), respectively represent strong-strong and strong-weak mineral interphases.

Calculated coefficients of variation in the elastic moduli of constituent mineral phases and the two polycrystalline granites are summarized in Table 1. All mineral phases show minor variability across the testing temperatures.

One-way ANOVA tests performed on both granites indicate statistically significant temperature effects: $F = 11.7$ for Utah and $F = 6.02$ for SURF, and $p < 0.001$ for both granites. For the quartz-albite (Q-A) interphase, one-way ANOVA followed by Tukey's Honestly Significant Difference post-hoc tests confirms that temperature has a significant effect on elastic modulus ($p < 0.001$), as shown in Fig. 6. In particular, the modulus at 100-400 °C is significantly higher than at 20-50 °C, for example, 20 °C vs 100-400 °C, $p < 0.05$, with the largest increases observed between 20 and 300 °C. In contrast, differences among the highest investigated temperatures, 200, 300, and 400 °C, are less distinguishable within the experimental scatter, indicating a high-temperature plateau where

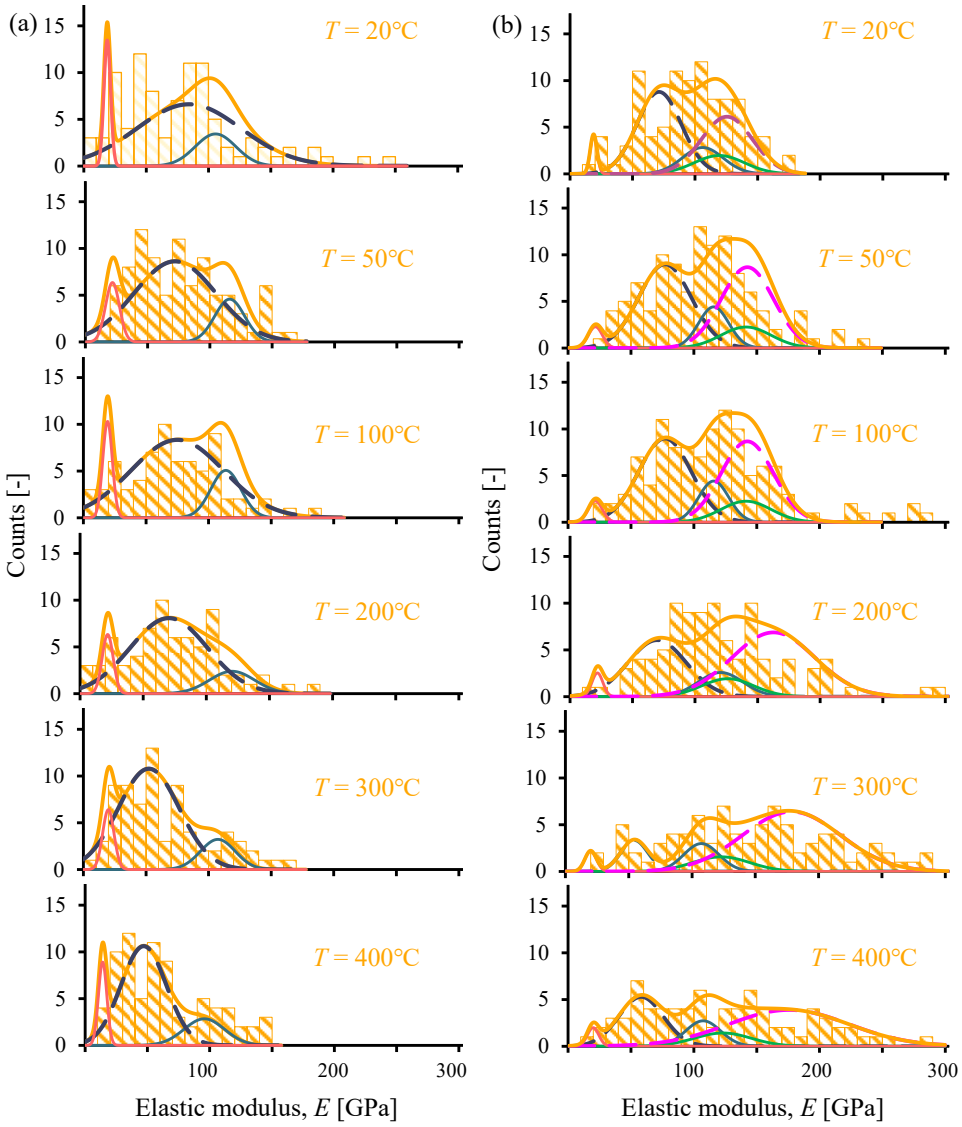

Fig. 5. Elastic moduli E distributions for (a) the SURF and (b) the Utah granites.

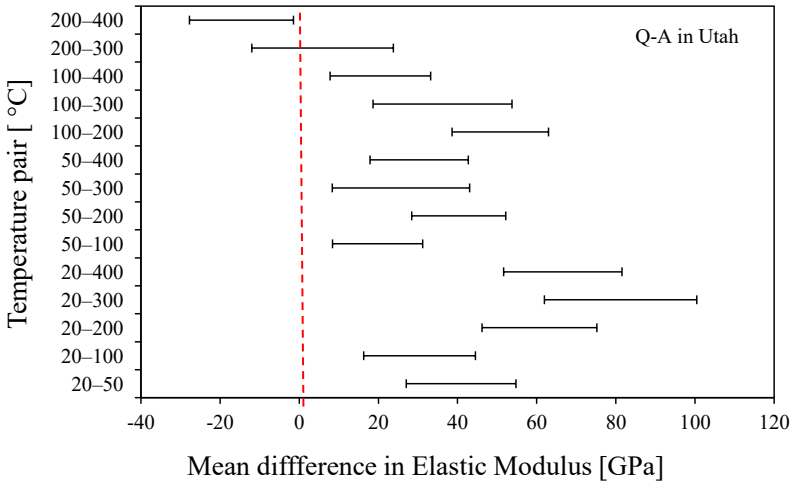

Fig. 6. Tukey's Honestly Significant Difference comparisons of the Q-A interphase modulus at varying temperature ranges.

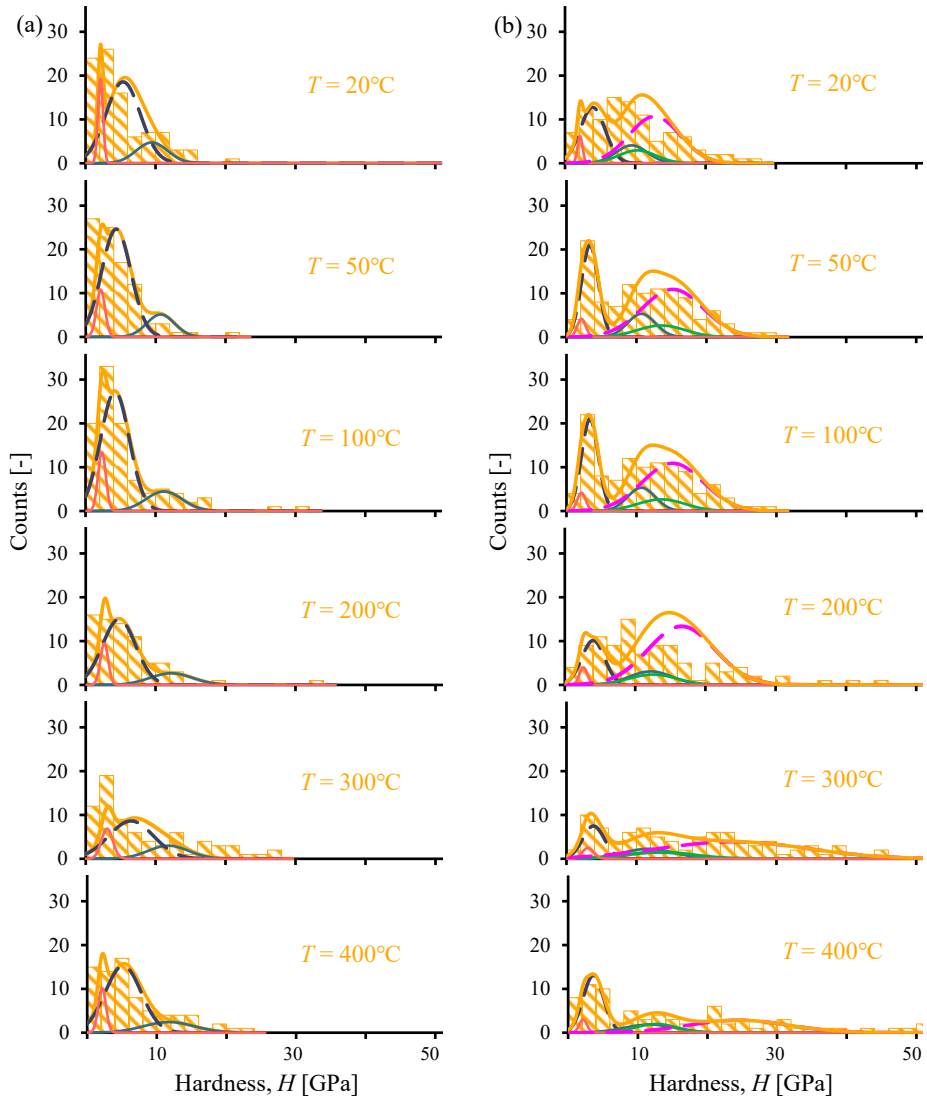

Fig. 7. Hardness H distributions for (a) the SURF and (b) the Utah granites.

additional heating produces only modest changes.

3.2 Temperature-dependent hardness variations

To contrast hardness distributions at different temperatures for the two tested granites, measured hardness data are presented in Fig. 7. They are also fitted using the Gaussian mixture model of constituent minerals and interphases in a similar manner as in Fig. 5. The results highlight that when the temperature reaches 300°C, both samples show clearly increased hardness, especially in the Utah sample. And the measured data captures the hardness of both intra- and inter-minerals, manifesting in multiple peaks corresponding to those of individual minerals (solid lines) and mineral-to-mineral (dashed lines) boundaries. Table 2 shows calculated data dispersion for the hardness of both constituent mineral phases and the two granites. All mineral phases show minor variability among the data obtained at the same testing temperatures.

3.3 Inter-mineral interfaces

Most previous studies offered the temperature-dependent behaviors of individual granitic minerals, yet not of inter-mineral interfaces. Therefore, Fig. 8(a) summarizes the temperature-dependent elastic modulus of both individual minerals and inter-mineral interfaces within the SURF and the Utah granite. The results show that the elastic moduli of individual minerals, as well as the soft-strong interphase Q-B (i.e., quartz-biotite or albite-biotite) in both samples, decrease with increasing temperature. The elastic modulus of the soft-strong interphase decreased from $\sim$ 83 GPa at 20 °C to $\sim$ 46.2 GPa at 400 °C (approximately 44% reduction) in the SURF granite, and from 70 to 53.3 GPa (approximately 24% reduction) in the Utah granite. Note that biotite has platy crystals and perfect cleavage at the basal plane. Its thermal expansion coefficient is around 17.3×10^{-6} and 9.65×10^{-6} K^{-1} along and normal to its c-axis (Hidnert and Dickson, 1945; Chon et al., 2003; Siegesmund et al., 2008); while that of the quartz is around

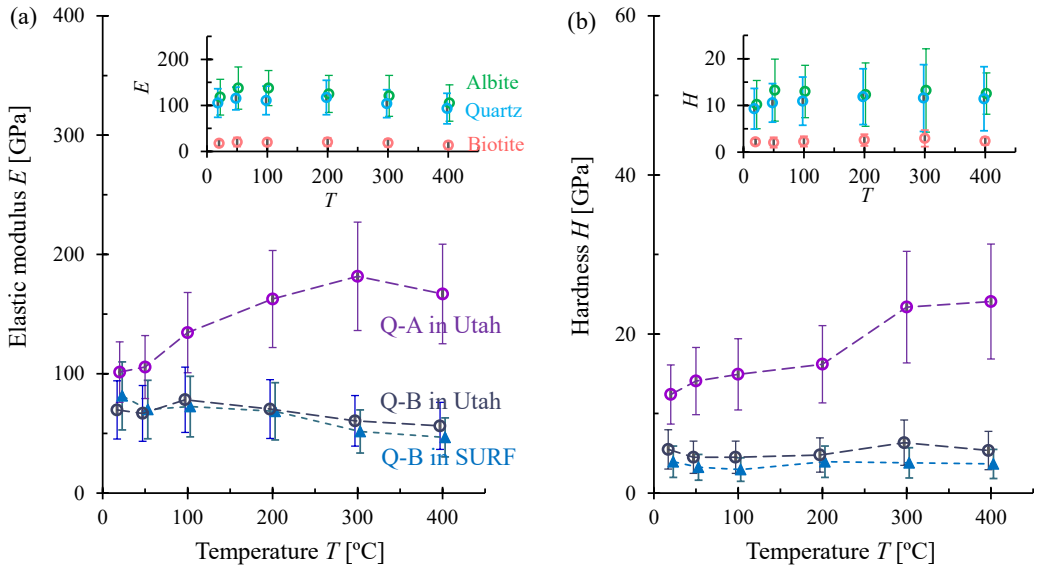

Fig. 8. Temperature-dependent (a) elastic modulus E and (b) hardness H of the interphases in the SURF and the Utah granites.

7.7×10^{-6} K^{-1} (Jerzy et al., 1999; Rüdrich, 2003; Siegesmund et al., 2008). Therefore, the reduced elastic modulus of the quartz-biotite and albite-biotite interphases may be attributed to structural degradation induced by excessive dilation of biotite.

Conversely, the elastic modulus of the strong-strong mineral interphase Q-A (i.e., quartz-albite) nearly doubled from ~ 99.3 GPa at 20 °C to ~ 180.5 GPa at 300 °C, and then decreased slightly to ~ 165.9 GPa at 400 °C (Fig. 8(a)). The results indicate that increasing temperature strengthens the interphase between minerals with similar mechanical and thermal properties, and that thermal expansion increases the apparent interphase elastic modulus, possibly by fracture closure and thermal stress accumulation. These temperature-dependent trends indicate that interphases do not simply behave as linear mixtures of constituent minerals, but instead exhibit a distinct strengthening behavior upon heating, particularly up to 300 °C, where mineral expansion caused closure of pre-existing cracks has been reported (Cooper and Simmons, 1977; Yang et al., 2017; Zhao and Feng, 2019). As temperature increases to 400 °C, however, thermal stresses may exceed mineral strength and cause damage that lowers the measured Q-A interphase stiffness through microcrack initiation and propagation. This interpretation is consistent with prior microstructural studies based on optical and SEM imaging of thermally treated granites, which show that microcracks preferentially initiate and propagate along quartz-feldspar interfaces, driven by tensile-compressive stress contrasts, which lead to decreased granite strength above 400-500 °C (Yang et al., 2017; Xu et al., 2023). As temperature increases further, and especially around 573 °C, acoustic emission and transport property measurements on quartz-bearing granites have shown that the most intense microcracking, as well as permeability and porosity changes coincide with the α-β quartz transition (Glover et al., 1995; Johnson et al., 2021). At even higher temperatures (e.g., 600-800 °C) pervasive intragranular cracking within quartz and feldspar begins to dominate the damage pattern (Gomah et al., 2024; Zhang et al., 2025). Therefore, the slight reduction in Q-A interphase modulus at 400 °C is interpreted as the onset of thermally induced damage at quartz-albite interfaces, rather than as a precursor effect of the α-β transition of quartz, whose degradation impacts would be expected only at temperatures beyond our experimental range.

Similarly, the measured hardness results (Fig. 8(b)) show that temperature increase has marginal impacts on the hardness of individual minerals and the strong-weak mineral interphase (approximately 4-5 GPa at all tested temperatures), but strengthens that of the strong-strong mineral interphase, which doubled from 12 GPa at 20 °C to 24 GPa at 400 °C.

The results in Fig. 8 clearly suggest that elevated temperatures cause predominantly inter-mineral changes, rather than intra-mineral. In the experiments performed in this study, granites were heated under dry, subsolidus conditions up to 400 °C, which is a range where similar experimental studies indicate that changes in mechanical properties are predominantly controlled by thermoelastic microcracking and evolution of pre-existing cracks rather than by extensive biotite dehydration or other mineralogical transformations (Chen et al., 2017; Qin et al., 2020; Xu et al., 2023; Li et al., 2024). Accordingly, the observed temperature-dependent variations in local modulus and hardness reflect crack closure and subsequent thermally induced microcracking at quartz-feldspar and quartz-biotite interfaces, with any dehydration, oxidation, or interfacial chemical reactions playing at most a secondary role under these conditions. As such, temperature increase up to 400 °C in this study induces marginal changes in the mechanical properties of biotite, reductions in those of quartz, albite, and strong-weak interphases (i.e., quartz-biotite and albite-biotite), but evident increase in that of the strong-strong interphase (i.e., quartz-albite) where strong minerals

show enhanced mineral interlocking as temperature increases (Liu et al., 2023). Therefore, the interphase of minerals with contrasting mechanical and thermal properties degrades with increasing temperature, yet the interphase of minerals with similar mechanical and thermal properties is strengthened by temperature. This explains previous findings that stress concentration tends to occur at mineral-to-mineral interphases, especially around stronger minerals (Vázquez et al., 2015). As temperature closes to 400 °C, interphases of strong minerals tend to show stress concentrations, and observed fractures were mostly inter-mineral around the biotite minerals and between quartz and feldspar (Xu et al., 2023).

3.4 Scale linkage between nano- and macro-mechanical behavior

The nanoindentation measurements reported here provide identification of local elastic modulus and hardness for individual minerals and mineral interphases, which can be interpreted as micromechanical building blocks for granitic rocks. The relatively high stiffness of quartz and albite, together with the strong-strong behavior of the Q-A interphase at moderate temperatures, is consistent with the observation that quartz- and feldspar-rich granites generally exhibit higher bulk elastic modulus and strength than rocks with weaker matrix phases (Lei et al., 2021; Lasheen et al., 2023). For example, nanoindentation and homogenization studies on granite have shown that quartz has the largest elastic modulus and hardness, followed by feldspar (intermediate) and mica (weakest), and that when these phase-scale properties are up-scaled, the predicted bulk elastic modulus agrees well with uniaxial compression tests (Lei et al., 2021; Lei et al., 2022). Such findings further validate other studies indicating that stiff quartz-feldspar frameworks control rock-scale stiffness (Hemmati et al., 2020; Lasheen et al., 2023). Laboratory tests on thermally treated granites further indicate that the uniaxial compressive strength and elastic modulus increase or remain relatively high up to about 200-300 °C due to thermal closure of grain-boundary microcracks, and then decrease as temperature rises beyond 300-400 °C as intergranular damage accumulates and microfractures coalesce to generate permeability and porosity changes (Yang et al., 2020; Zhang et al., 2022; Meng et al., 2026). This pattern of an initial strength increase followed by deterioration at higher temperatures is consistent with a transition between inter-mineral microcrack-closure mechanisms at low-moderate temperatures and damage-dominated behavior at elevated temperatures, as presented in this study. More specifically, the nanoindentation-derived behavior of the Q-A interphase in this study also shows an initial strengthening with temperature up to 300 °C, followed by a slight reduction in interphase stiffness at 400 °C, which is interpreted as the onset of thermally induced microcracking that contributes to bulk modulus and strength loss at the rock scale.

3.5 Limitations and future work

The isolation of the potential indentation rate-dependent effects across minerals and temperatures is a limitation of this study. Because different minerals (e.g., quartz, albite and biotite) exhibit distinct thermal dilation behaviors, the influence of nanoindentation loading rate as a function of mineral type and temperature will be examined in future work to evaluate how these effects deviate from the baseline established here. Additionally, the effects of more complex loading paths such as cyclic or fatigue loading, which were beyond the scope of this work, will be investigated in a subsequent study.

In addition to different mineralogy, the two tested granites were from different in situ temperatures and stresses (i.e., depths). The deeper Utah core experienced higher in-situ confining stress and temperature, which would tend to keep grain-boundary cracks closed, whereas the shallower SURF core may carry a higher density of stress-relief and cooling microcracks. This is consistent with, and indeed helps explain, the greater compliance and higher coefficient of variation observed in the SURF sample (Table 1 and Fig. 2). Because all specimens were re-equilibrated and tested at controlled setpoints from 20 °C to 400 °C, and because both samples were taken well below their respective in-situ temperatures at the lowest test step, neither sample was tested only above its native temperature. The 45 and 112 °C in-situ values therefore bracket the lower end of our test range and do not bias the high-temperature (200-400 °C) trends that drive our conclusions. Note also that the difference in biotite content (i.e., 38.8% in SURF vs. 11.4% in Utah) is far larger than any plausible effect of the depth or temperature difference, and it is precisely this mineralogical contrast that produces the opposite thermal responses of net weakening vs. net strengthening predicted by our interphase mechanism.

4. Conclusions

Fundamental mechanical properties of granite samples obtained from enhanced geothermal systems sites have been tested using instrumented nanoindentation in temperatures ranging from 20 to 400 °C. This study resolves the mechanical properties as a function of temperature for individual granitic minerals and their interphases in situ, at temperature, rather than on thermally-treated-then-cooled specimens, thereby preserving the thermal expansion and interphase stresses that govern the high-temperature response. The results explain intra- and inter-mineral behaviors upon heating and offer mechanistic understandings of temperature-dependent granite properties at the grain scale. The salient conclusions of this study follow.

- Temperature causes predominantly inter-mineral rather than intra-mineral changes in granite. Temperature increase induces relatively marginal changes in the mechanical properties of biotite, and more evidently degrades the mechanical properties of quartz and albite. Whereas, the most pronounced changes occur at the mineral interphases.
- The interphase of minerals with contrasting strengths and coefficients of thermal expansion, like quartz-biotite and albite-biotite, degrades with increasing temperature. Conversely, the interphase of minerals with similar mechanical and thermal properties, like quartz-albite, is strengthened by temperature possibly due to fracture

closure and thermal stress accumulation.

- Granite properties at elevated temperatures are competing results between thermal degradation in mismatching mineral interphases and thermal strengthening of interphases of minerals with comparable properties. This leads to an overall thermal degradation in the SURF granite due to high biotite content and thermal strengthening in the Utah granite due to high quartz and albite content.
- Elevated temperatures increase the hardness of both tested granite samples, more evidence increase in the Utah granite. This implies that elevated temperature (especially >300°C for superhot conditions) increases the difficulties in drilling through the tested samples.
- These interphase-controlled mechanisms reconcile the long-standing controversy over whether granite weakens or strengthens upon heating: the net response of a given granite is set by which interphase type dominates its mineral assemblage. Practically, this implies that thermal strengthening, and the associated increase in interphase hardness observed in the quartz- and albite-rich Utah granite, can raise the difficulty of drilling through such rocks at elevated temperature, whereas biotite-rich granites such as SURF are expected to weaken.

Acknowledgements

This material is based upon work supported by the National Science Foundation (Nos. CMMI1943722, CMMI-2416332, IRES-1854030, and EAR-2433040). Any opinions, findings and conclusions, or recommendations expressed in this material are those of the authors and do not necessarily reflect those of the NSF.

Conflicts of interest

The authors declare no competing interest.

References

American Society for Testing and Materials(ASTM). Standard Practice for Instrumented Indentation Testing: E2546-07. ASTM International, 2007.

Atkinson, B. K. Stress corrosion and the rate-dependent tensile failure of a fine-grained quartz rock. Tectonophysics, 1980, 65(3): 281-290.

Chen, Y. -L., Ni, J., Shao, W., et al. Experimental study on the influence of temperature on the mechanical properties of granite under uni-axial compression and fatigue loading. International Journal of Rock Mechanics and Mining Sciences, 2012, 56: 62-66.

Chen, Y. -L., Wang, S. -R., Ni, J., et al. An experimental study of the mechanical properties of granite after high temperature exposure based on mineral characteristics. Engineering Geology, 2017, 220: 234-242.

Chon, C. -M., Kim, S. A., Moon, H. -S. Crystal structures of biotite at high temperatures and of heat-treated biotite using neutron powder diffraction. Clays and Clay Minerals, 2003, 51(5): 519-528.

Cooper, H., Simmons, G. The effect of cracks on the thermal expansion of rocks. Earth and Planetary Science Letters, 1977, 36(3): 404-412.

Darot, M., Gueguen, Y., Baratin, M. L. Permeability of thermally cracked granite. Geophysical Research Letters, 1992, 19(9): 869-872.

David, C., Menéndez, B., Darot, M. Influence of stress-induced and thermal cracking on physical properties and microstructure of la peyratte granite. International Journal of Rock Mechanics and Mining Sciences, 1999, 36(4): 433-448.

David, E. C., Brantut, N., Schubnel, A., et al. Sliding crack model for nonlinearity and hysteresis in the uniaxial stress-strain curve of rock. International Journal of Rock Mechanics and Mining Sciences, 2012, 52: 9-17.

Dwivedi, R. D., Goel, R. K., Prasad, V. V. R., et al. Thermo-mechanical properties of indian and other granites. International Journal of Rock Mechanics and Mining Sciences, 2008, 45(3): 303-315.

Espinoza, W. F., Pereira, J. -M., Kneafsey, T., et al. Mechanical and creep properties of granitic minerals of albite, biotite, and quartz at elevated temperature. Geomechanics for Energy and the Environment, 2023, 34: 100465.

Espinoza, W. F., Zhang, F., Dai, S. Impacts of temperature on the mechanical properties of longmaxi shale outcrops using instrumented nanoindentation. Geomechanics for Energy and the Environment, 2022, 30: 100348.

Feng, G., Kang, Y., Wang, X. -C. Fracture failure of granite after varied durations of thermal treatment: An experimental study. Royal Society Open Science, 2019, 6(7): 190144.

Gautam, P. K., Verma, A. K., Jha, M. K., et al. Effect of high temperature on physical and mechanical properties of jalore granite. Journal of Applied Geophysics, 2018, 159: 460-474.

Géraud, Y., Mazerolle, F., Raynaud, S. Comparison between connected and overall porosity of thermally stressed granites. Journal of Structural Geology, 1992, 14(8): 981-990.

Gibb, F. G., Attrill, P. G. Granite recrystallization: The key to the nuclear waste problem? Geology, 2003, 31(8): 657-660.

Glatz, J. P., Toscano, E. H., Paghosa, G., et al. Influence of granite on the leaching behaviour of different nuclear waste forms. Journal of Nuclear Materials, 1995, 223(1): 84-89.

Glover, P., Baud, P., Darot, M., et al. A/β phase transition in quartz monitored using acoustic emissions. Geophysical Journal International, 1995, 120(3): 775-782.

Gomah, M. E., Li, G., Omar, A. A., et al. Thermal-induced microstructure deterioration of egyptian granodiorite and associated physico-mechanical responses. Materials, 2024, 17(6): 1305.

Gómez-Heras, M., Smith, B. J., Fort, R. Influence of surface heterogeneities of building granite on its thermal response and its potential for the generation of thermoclasty.

Environmental Geology, 2008, 56(3): 547.

Griffiths, L., Lengliné, O., Heap, M. J., et al. Thermal cracking in westerly granite monitored using direct wave velocity, coda wave interferometry, and acoustic emissions. Journal of Geophysical Research: Solid Earth, 2018, 123(3): 2246-2261.

Hamdi, P., Stead, D., Elmo, D. Characterizing the influence of stress-induced microcracks on the laboratory strength and fracture development in brittle rocks using a finite-discrete element method-micro discrete fracture network fdem-μdfn approach. Journal of Rock Mechanics and Geotechnical Engineering, 2015, 7(6): 609-625.

Hemmati, A., Ghafoori, M., Moomivand, H., et al. The effect of mineralogy and textural characteristics on the strength of crystalline igneous rocks using image-based textural quantification. Engineering Geology, 2020, 266: 105467.

Hidnert, P., Dickson, G. Some physical properties of mica. Research of the National Bureau of Standards, 1945, 35: 309-353.

Hill, B., Rogers, T., Herter, J., et al. Superhot rock energy: A vision for firm, global zero-carbon energy. USA, Clean Air Task Force Report, 2022.

Hu, J., Sun, Q., Pan, X. Variation of mechanical properties of granite after high-temperature treatment. Arabian Journal of Geosciences, 2018, 11(2): 43.

Inserra, C., Biwa, S., Chen, Y. Influence of thermal damage on linear and nonlinear acoustic properties of granite. International Journal of Rock Mechanics and Mining Sciences, 2013, 62: 96-104.

Jerzy, K., Krzysztof, D., Michael, T., et al. Complex permittivity of some ultralow loss dielectric crystals at cryogenic temperatures. Measurement Science and Technology, 1999, 10(5): 387.

Johnson, S. E., Song, W. J., Cook, A. C., et al. The quartz $\alpha \leftrightarrow \beta$ phase transition: Does it drive damage and reaction in continental crust? Earth and Planetary Science Letters, 2021, 553: 116622.

Kim, J. -Y., Lee, J. -J., Lee, Y. -H., et al. Surface roughness effect in instrumented indentation: A simple contact depth model and its verification. Journal of Materials Research, 2006, 21(12): 2975-2978.

Korte, S., Stearn, R. J., Wheeler, J. M., et al. High temperature microcompression and nanoindentation in vacuum. Journal of Materials Research, 2012, 27(1): 167-176.

Kranz, R. L. Microcracks in rocks: A review. Tectonophysics, 1983, 100(1): 449-480.

Kumari, W. G. P., Beaumont, D. M., Ranjith, P. G., et al. An experimental study on tensile characteristics of granite rocks exposed to different high-temperature treatments. Geomechanics and Geophysics for Geo-Energy and Geo-Resources, 2019, 5(1): 47-64.

Kumari, W. G. P., Ranjith, P. G., Perera, M. S. A., et al. Temperature-dependent mechanical behaviour of australian strathbogie granite with different cooling treatments. Engineering Geology, 2017, 229: 31-44.

Lan, H., Martin, C. D., Hu, B. Effect of heterogeneity of brittle rock on micromechanical extensile behavior during compression loading. Journal of Geophysical Research: Solid Earth, 2010, 115(B1): B01202.

Lasheen, E. S. R., Rashwan, M. A., Azer, M. K. Effect of mineralogical variations on physico-mechanical and thermal properties of granitic rocks. Scientific Reports, 2023, 13(1): 10320.

Lei, M., Dang, F. -N., Xue, H., et al. Evaluation method of granite multiscale mechanical properties based on nanoindentation technology. Geofluids, 2021, 2021: 6745900.

Lei, M., Dang, F. -N., Xue, H., et al. Study on the effect of nanoindentation test method on micromechanical properties of granite minerals. Geofluids, 2022, 2022: 5834979.

Li, C., Feng, G., Zhang, X., et al. Study on the failure mechanism of high-temperature granite under two cooling modes. Scientific Reports, 2024, 14(1): 15630.

Li, M., Wu, Z., Weng, L., et al. Quantitative relationships between the mineral composition and macro mechanical behaviors of granite under different temperatures: Insights from mesostructure-based dem investigations. Computers and Geotechnics, 2022, 148: 104838.

Lin, W. Permanent strain of thermal expansion and thermally induced microcracking in inada granite. Journal of Geophysical Research: Solid Earth, 2002, 107(B10): 2215.

Liu, J.-F., Luo, X., Feng, G., et al. Creep characteristics of thermally-stressed beishan granite under triaxial compression. International Journal of Rock Mechanics and Mining Sciences, 2023, 162: 105302.

Martin, C. D., Stimpson, B. The effect of sample disturbance on laboratory properties of lac du bonnet granite. Canadian Geotechnical Journal, 1994, 31(5): 692-702.

Meng, M., Pyatina, T., Kibikas, W., et al. Review of experimental and numerical approaches to wellbore material performance under supercritical geothermal conditions. Paper SGP-TR-229 Presented at the Stanford Geothermal Workshop, Stanford, CA, 9-11 February, 2026.

Merriam, R., Rieke Iii, H. H., Kim, Y. C. Tensile strength related to mineralogy and texture of some granitic rocks. Engineering Geology, 1970, 4(2): 155-160.

Michałek, J., Pachnicz, M., Sobótka, M. Application of nanoindentation and 2D and 3D imaging to characterise selected features of the internal microstructure of spun concrete. Materials, 2019, 12(7): 1016.

Miskovsky, K., Taborda Duarte, M., Kou, S. Q., et al. Influence of the mineralogical composition and textural properties on the quality of coarse aggregates. Journal of Materials Engineering and Performance, 2004, 13(2): 144-150.

Nasseri, M., Schubnel, A., Young, R. Coupled evolutions of fracture toughness and elastic wave velocities at high crack density in thermally treated westerly granite. International Journal of Rock Mechanics and Mining Sciences, 2007, 44(4): 601-616.

Oliver, Pharr, G. Measurement of hardness and elastic modulus by instrumented indentation: Advances in understanding and refinements to methodology. Journal of Materials Research, 2004, 19(1): 3-20.

Oliver, W. C., Pharr, G. M. An improved technique for determining hardness and elastic modulus using load and

displacement sensing indentation experiments. Journal of Materials Research, 1992, 7(6): 1564-1583.

Peng, J., Yang, S. -Q. Comparison of mechanical behavior and acoustic emission characteristics of three thermally-damaged rocks. Energies, 2018, 11(9): 2350.

Qin, Y., Tian, H., Xu, N. -X., et al. Physical and mechanical properties of granite after high-temperature treatment. Rock Mechanics and Rock Engineering, 2020, 53(1): 305-322.

Rüdrich, J. M. Gefügekontrollierte verwitterung natürlicher und konservierter marmore. Geottingen, Georg-August-Universitaet Goettingen, 2003.

Saksala, T. Numerical modeling of temperature effect on tensile strength of granitic rock. Applied Sciences, 2021, 11(10): 4407.

Shao, S., Ranjith, P. G., Wasantha, P. L. P., et al. Experimental and numerical studies on the mechanical behaviour of australian strathbogie granite at high temperatures: An application to geothermal energy. Geothermics, 2015, 54: 96-108.

Sharma, A., Ouyang, M., Hintsala, E., et al. High-temperature nanoindentation creep studies on castable and sintered nanostructured low-activation ferritic-martensitic alloys. Journal of Nuclear Materials, 2025, 611: 155804.

Shea, W. T., Kronenberg, A. K. Strength and anisotropy of foliated rocks with varied mica contents. Journal of Structural Geology, 1993, 15(9): 1097-1121.

Siegesmund, S., Mosch, S., Scheffzük, C., et al. The bowing potential of granitic rocks: Rock fabrics, thermal properties and residual strain. Environmental Geology, 2008, 55(7): 1437-1448.

Singh, B., P.G, R., Chandrasekharam, D., et al. Thermo-mechanical properties of bundelkhand granite near jhansi, india. Geomechanics and Geophysics for Geo-Energy and Geo-Resources, 2015, 1(1): 35-53.

Sun, Q., Zhang, W., Xue, L., et al. Thermal damage pattern and thresholds of granite. Environmental Earth Sciences, 2015, 74(3): 2341-2349.

Talukdar, M., Guha Roy, D., Singh, T. N. Correlating mode-i fracture toughness and mechanical properties of heat-treated crystalline rocks. Journal of Rock Mechanics and Geotechnical Engineering, 2018, 10(1): 91-101.

Török, A., Török, Á. The effect of temperature on the strength of two different granites. Central European Geology, 2015, 58: 356-369.

Vázquez, P., Shushakova, V., Gómez-Heras, M. Influence of mineralogy on granite decay induced by temperature increase: Experimental observations and stress simulation. Engineering Geology, 2015, 189: 58-67.

Wang, F., Konietzky, H. Thermal cracking in granite during a heating–cooling cycle up to 1000 °C: Laboratory testing and real-time simulation. Rock Mechanics and Rock Engineering, 2022, 55(3): 1411-1428.

Wang, H. F., Bonner, B. P., Carlson, S. R., et al. Thermal stress cracking in granite. Journal of Geophysical Research: Solid Earth, 1989, 94(B2): 1745-1758.

Wang, X. -Q., Schubnel, A., Fortin, J., et al. Physical properties and brittle strength of thermally cracked granite under confinement. Journal of Geophysical Research: Solid Earth, 2013, 118(12): 6099-6112.

Wong, L. N. Y., Zhang, Y., Wu, Z. Rock strengthening or weakening upon heating in the mild temperature range? Engineering Geology, 2020, 272: 105619.

Wyborn, D., De Graaf, L., Davidson, S., et al. Development of australia's first hot fractured rock (HFR) underground heat exchanger, cooper basin, south australia. Paper Presented at PESA Eastern Australian Basin Symposium II, Adelaide, Australia, 19-22 September, 2004.

Xu, J., Zhang, Y., Rutqvist, J., et al. Thermally induced microcracks in granite and their effect on the macroscale mechanical behavior. Journal of Geophysical Research: Solid Earth, 2023, 128(1): e2022JB024920.

Xu, X. L., Karakus, M. A coupled thermo-mechanical damage model for granite. International Journal of Rock Mechanics and Mining Sciences, 2018, 103: 195-204.

Yang, S. -Q., Ranjith, P., Jing, H. -W., et al. An experimental investigation on thermal damage and failure mechanical behavior of granite after exposure to different high temperature treatments. Geothermics, 2017, 65: 180-197.

Yang, S. -Q., Tian, W. -L., Elsworth, D., et al. An experimental study of effect of high temperature on the permeability evolution and failure response of granite under triaxial compression. Rock Mechanics and Rock Engineering, 2020, 53(10): 4403-4427.

Yin, T. -b., Shu, R. -h., Li, X.-b., et al. Comparison of mechanical properties in high temperature and thermal treatment granite. Transactions of Nonferrous Metals Society of China, 2016, 26(7): 1926-1937.

Yin, T., Wu, Y., Li, Q., et al. Determination of double-k fracture toughness parameters of thermally treated granite using notched semi-circular bending specimen. Engineering Fracture Mechanics, 2020, 226: 106865.

Zhang, F., Zhao, J., Hu, D., et al. Laboratory investigation on physical and mechanical properties of granite after heating and water-cooling treatment. Rock Mechanics and Rock Engineering, 2018, 51(3): 677-694.

Zhang, J., Hu, Z., Liu, D., et al. Thermal-induced damage mechanisms and permeability evolution in gneiss for deep mining applications. Frontiers in Earth Science, 2025, 13: 1603348.

Zhang, Y., Zhang, F., Yang, K., et al. Effects of real-time high temperature and loading rate on deformation and strength behavior of granite. Geofluids, 2022, 2022: 9426378.

Zhao, P., Feng, Z.-J. Thermal deformation of granite under different temperature and pressure pathways. Advances in Materials Science and Engineering, 2019, 2019: 7869804.

Zhao, Z., Zhao, X. Thermally-induced microcracking in granites: Insights from sem observation and dem modeling. Paper Presented at ISRM International Symposium-10th Asian Rock Mechanics Symposium, Singapore, 29 October-3 November, 2018.

Zhou, Y., Wu, Z., Weng, L., et al. Seepage characteristics of chemical grout flow in porous sandstone with a fracture under different temperature conditions: An nmr based experimental investigation. International Journal of Rock Mechanics and Mining Sciences, 2021, 142: 104764.